

Imaging of ferroelectric polarization in $\text{Pb}(\text{Mg}_{1/3}\text{Nb}_{2/3})\text{O}_3\text{-PbTiO}_3$ crystals by scanning electro-optic microscopy

O. Tikhomirov^{a)}

PolyLab CNR-INFM, Largo Bruno Pontecorvo 3, 56127 Pisa, Italy and Institute of Solid State Physics, Chernogolovka, Moscow 142432, Russia

M. Labardi

PolyLab CNR-INFM, Largo Bruno Pontecorvo 3, 56127 Pisa, Italy

C. Ascoli

Dipartimento di Fisica "Enrico Fermi," Università di Pisa, Largo Bruno Pontecorvo 3, 56127 Pisa, Italy

M. Allegrini

Dipartimento di Fisica "Enrico Fermi," Università di Pisa, Largo Bruno Pontecorvo 3, 56127 Pisa, Italy and PolyLab CNR-INFM, Largo Bruno Pontecorvo 3, 56127 Pisa, Italy

L. Lebrun

LGEF, INSA de Lyon, 8 rue de la Physique, 69621 Villeurbanne, France

(Received 21 November 2005; accepted 13 February 2006; published online 14 April 2006)

Spatial distribution of the ferroelectric polarization in $(1-x)\text{Pb}(\text{Mg}_{1/3}\text{Nb}_{2/3})\text{O}_3-x\text{PbTiO}_3$ single crystals with $x=0.25$ has been visualized using scanning confocal electro-optic microscopy. Domains showing different values and signs of the linear electro-optic effect are observed in both $\langle 001 \rangle$ and $\langle 111 \rangle$ oriented crystal plates in case of application of a symmetry-breaking dc electric field. Features of the observed images are explained on the basis of the electro-optic tensor analysis. © 2006 American Institute of Physics. [DOI: [10.1063/1.2190907](https://doi.org/10.1063/1.2190907)]

The $\text{Pb}(\text{Mg}_{1/3}\text{Nb}_{2/3})\text{O}_3\text{-PbTiO}_3$ (PMN-PT) system attracts attention due to promising dielectric,¹ piezoelectric,² and electro-optic³ (EO) properties caused mainly by its phase diagram features, namely, the relaxor state¹ and the morphotropic phase boundary (MPB).⁴ Both these phenomena involve some kind of spatial inhomogeneity. In relaxors, fluctuations of chemical composition, nanopolar domains, or local built-in internal electric fields are considered as likely cause of the observed diffused peak of dielectric permittivity.⁵ For compositions close to MPB, the lattice instability model allowing rotation of the ferroelectric (FE) polarization⁶ competes with extrinsic effect from walls separating tetragonal, rhombohedral, and monoclinic⁷ domains. The spatially resolved techniques are expected to provide the decisive arguments in these discussions.

Two experimental techniques generally used to reveal the domain structure of PMN-PT are polarized optical microscopy^{8,9} (POM) and piezoelectric force microscopy (PFM).¹⁰⁻¹⁴ However, POM is restricted in spatial resolution and contrast, while PFM involves highly inhomogeneous electric field. We propose to visualize the domain structure with another alternative tool: scanning confocal optical microscopy (CSOM) with EO modulation.¹⁵ This technique has given good results with FE single crystals¹⁶ as well as with thin films.¹⁷ Important advantages of this microscopy are relatively low gradient of probing electric field and effective EO contrast between different phases or directions of the FE polarization.¹⁶ In this Letter we report visualization of the domain structure of the $(1-x)\text{PMN}-x\text{PT}$ crystals with $x=0.25$ using diffraction-limited modulated CSOM.

The PMN-25 mol % PT single crystals were grown using Bridgman technique from columbite precursor

MgNb_2O_5 . PMN-PT batches were weighed out with excess of 1 mol % PbO. The powders were pressed at 1 ton/cm² using polyvinyl alcohol (PVA) binder into 25 mm diameter and 10 mm length compacts. After binder burnout, the compacts were sintered at 1250 °C for 4 h in sealed alumina crucibles with PbZrO_3 packing powder to suppress the volatilization of lead in compacts. Compacts were put into a sealed Y shape platinum crucible to prevent the evaporation of lead during the growth. After soaking for 4 h at 1450 °C, the crucible was then allowed to pull down at a rate of 1 mm/h through a maximum thermal gradient of around 30 °C/cm at the growth interface. Single crystals were oriented along pseudocubic $\langle 001 \rangle$ or $\langle 111 \rangle$ direction with an accuracy less than 0.5° using x-ray diffraction. The surfaces of samples with typical dimensions of $8 \times 8 \times 1$ mm³ were polished using 1 μm diamond compound. The pairs of stripe electrodes with 200–300 μm spacing have been painted on the surface with silver paste in arbitrary direction to provide application of both ac and dc electric fields from a high voltage amplifier.

The scanning confocal microscope is similar to the setup described in Ref. 16. The high numerical aperture (NA = 0.8) objective is filled by 633 nm laser light passed through a spatial filter and a beam expander. The raster scanning is produced by a 90° pair of galvanometrically controlled mirrors placed above the objective. The light reflected from the crystal surface passes back through the objective and spatial filter to be registered by a balanced photodetector. The map of intensity of reflected light corresponds to the conventional optical image, while the picture formed by point-to-point measurements of the modulated in-phase signal from a lock-in amplifier at the frequency of ac electric field, applied to the crystal, presents the linear EO image. Both optical and EO pictures are acquired simultaneously.

^{a)}Electronic mail: tikhom@df.unipi.it

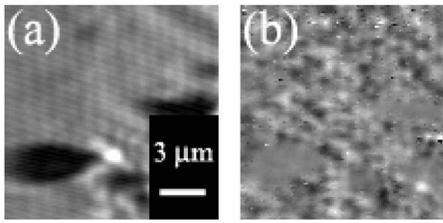


FIG. 1. Optical (a) and electro-optic (b) images of the $\langle 001 \rangle$ surface of the PMN-PT crystal after application of the dc bias voltage of -50 V.

Figure 1(a) reproduces the optical picture obtained from the $\langle 001 \rangle$ PMN-PT crystal. The reflected light is fairly homogeneous along the surface except for relatively weak (up to 10%–15%) variations of the intensity caused by structural features on the surface. The optical picture remains visually unaffected during and after application of both ac and dc electric fields.

Before any electric treatment, EO signal is null across the whole sample. This correlates with the earlier PFM observation on a similar material where only separate nanoscopic domains much smaller than optical wavelength have been found.¹⁸ We have observed, nevertheless, that application of moderate dc field induced irreversible formation of the microscopic electro-optically active regions throughout the crystal. Figure 1(b) shows the EO image of the same part of the crystal after application of the dc voltage of 50 V. Numerous regions of both positive (bright) and negative (dark areas) responses can be seen, as well as areas with zero ac signal, corresponding either to local paraelectric state or to special directions of FE polarization.¹⁹ Some of the domains in the EO image can be linked to structural features seen in the optical image, too [Fig. 1(a)]; for example, the dark lens-shaped area in the optical image provides no EO response. However, most FE domains, well seen in the EO mode of observation, show no optical contrast.

The $\langle 111 \rangle$ samples give qualitatively similar pictures. No ac signal was obtained from virgin crystals [Fig. 2(a)], but the domain structure arises starting from some critical dc voltage, positive [Fig. 2(b)] or negative, and becomes stable in a higher field [Fig. 2(c)]. The shape of domains is a little bit different comparing with $\langle 001 \rangle$ samples, featuring elongated domains, often accompanied by adjacent stripes of opposite sign. EO contrast, in general, is higher than for $\langle 001 \rangle$. Stability of the domain pattern is proved by diminishing the bias voltage back to its previous value [Fig. 2(d)] and further to zero [Fig. 2(e)]. Reversal of the field sign results in minor changes of this domain structure, mainly in orientation of the stripe domains and overall decrease of the EO contrast [Fig. 2(f)]. This structure remains approximately unchanged down to -100 V and back to positive values [Fig. 2(g)] where the pattern “written” by high positive voltage reappears [Fig. 2(h)].

The observed lack of symmetry of the domain behavior in negative and positive fields is apparently due to the high bias field applied during initial coalescence of invisible (at CSOM resolution) nanodomains into microscopic domain structure. The “shifted” configuration of FE polarization results in a kind of built-in internal bias field (like at biased ferroelectric phase transition). The domain structure in $\langle 001 \rangle$ samples looks to be even less affected by the field variations. Though some isolated spots can change their shape or disappear, the whole picture remains approximately the same de-

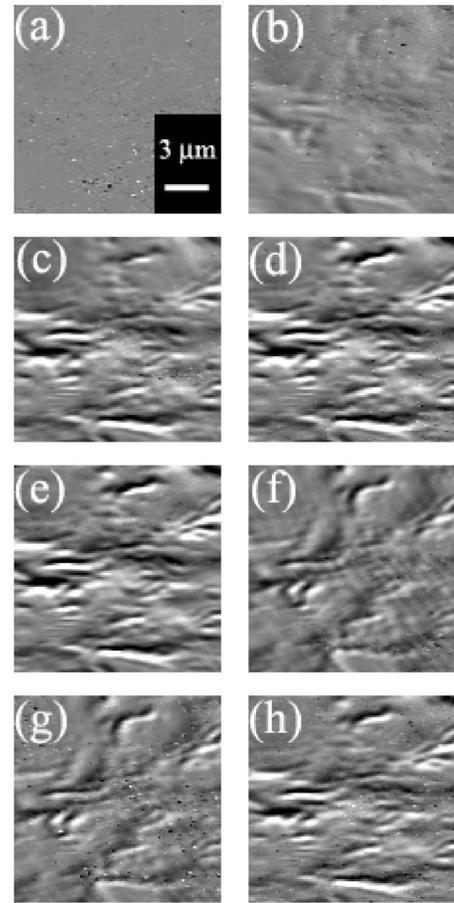


FIG. 2. Evolution of the domain structure in the $\langle 111 \rangle$ crystal during application and variation of the external dc bias: (a) $+35$ V, (b) $+70$ V, (c) $+100$ V, (d) $+70$ V, (e) 0 V, (f) -35 V, (g) $+35$ V, and (h) $+100$ V.

spite changes of the dc electric field value or its reversal.

The EO response produced by a FE can be determined considering the EO tensor.¹⁶ Composition $x=0.25$ is situated near the boundary between the (macroscopically) pseudocubic $m3m$ phase, giving no linear EO effect, and the FE rhombohedral $3m$ phase polarized along $\langle 111 \rangle$. The latter symmetry is the same as for LiNbO_3 already studied with CSOM.¹⁶ Though the numerical analysis performed in Ref. 16 cannot be applied directly to PMN-PT due to lack of the full set of EO constants,²⁰ qualitative explanation can be given to observed EO contrast and switching behavior. Both $\langle 001 \rangle$ and $\langle 111 \rangle$ samples can bear FE polarization at some angle to the surface only. The in-plane electric field affects mainly the horizontal component. There are eight possible directions of FE polarization having the same angle with a $\langle 001 \rangle$ plane; the in-plane components differ by angles of 90° or 180° between them. The driving force at the domain walls is relatively weak due to the small in-plane component of the polarization. Moreover, in general the field will affect some pairs of domains more and the other ones less, making the whole domain pattern stiffer. Due to these reasons we can expect weak response to the switching field in $\langle 001 \rangle$ samples as observed. Further, mainly the out-of-plane FE component should have small EO response to the in-plane field, similar to out-of-plane regions in thin films.¹⁹

The eight directions of FE polarization in the $\langle 111 \rangle$ sample are not equivalent: there is one pair normal to the surface (not affected by the in-plane field), and six other

directions lying very close to the surface plane with 60° symmetry. The in-plane switching between them is much easier comparing with $\langle 001 \rangle$. The EO contrast in this configuration is high, similar to in-plane domains in FE films,¹⁹ also in good agreement with Fig. 2.

In brief, we have visualized the inhomogeneous FE polarization pattern in PMN–PT crystals using EO CSOM. We observed appearance of the microscopic scale domains from initially quasihomogeneous state under the action of dc electric bias field and their further evolution with variations of this field. The obtained data are in good agreement with observations provided by PFM (Ref. 18) and with qualitative analysis of the EO tensor.

This research was supported by a Marie Curie International Fellowship within the sixth European Commission Framework Programme, Contract No. MIF CT 2004 002557, and by the Fondazione Cassa di Risparmio di Pisa.

¹Z.-Y. Cheng, R. S. Katiyar, X. Yao, and A. Guo, *Phys. Rev. B* **55**, 8165 (1997).

²S.-E. Park and T. R. Shrout, *J. Appl. Phys.* **82**, 1804 (1997).

³Y. Lu, G.-H. Gin, M. Cronin-Golomb, S.-W. Liu, H. Jiang, F.-L. Wang, J.

Zhao, S.-Q. Wang, and A. J. Drehman, *Appl. Phys. Lett.* **72**, 2927 (1998).

⁴O. Noblanc, P. Gaucher, and G. Calvarin, *J. Appl. Phys.* **79**, 4291 (1996).

⁵L. E. Cross, *Ferroelectrics* **76**, 241 (1987).

⁶H. Fu and R. E. Cohen, *Nature (London)* **403**, 281 (2000).

⁷B. Noheda, D. E. Cox, G. Shirane, J. A. Gonzalo, L. E. Cross, and S.-E. Park, *Appl. Phys. Lett.* **74**, 2059 (1999).

⁸Z.-G. Ye and M. Dong, *J. Appl. Phys.* **87**, 2312 (2000).

⁹C.-S. Tu, C.-L. Tsai, V. Hugo Schmidt, H. Luo, and Z. Yin, *J. Appl. Phys.* **89**, 7908 (2001).

¹⁰M. Abplanalp, D. Barošová, P. Bridenbaugh, J. Erhart, J. Fousek, P. Günter, J. Nosek, and M. Šulc, *J. Appl. Phys.* **91**, 3797 (2002).

¹¹F. Bai, J. Li, and D. Viehland, *Appl. Phys. Lett.* **85**, 4457 (2004).

¹²V. V. Shvartsman and A. L. Kholkin, *Phys. Rev. B* **69**, 014102 (2004).

¹³H. F. Yu, H. R. Zeng, H. X. Wang, G. R. Li, H. S. Luo, and Q. R. Yin, *Solid State Commun.* **133**, 311 (2005).

¹⁴X. Zhao, J. Y. Dai, J. Wang, H. L. W. Chan, C. L. Choy, X. M. Wand, and H. S. Luo, *J. Appl. Phys.* **97**, 094107 (2005).

¹⁵C. Hubert, J. Levy, A. C. Carter, W. Chang, S. W. Kiechoever, J. S. Horwitz, and D. B. Chrisey, *Appl. Phys. Lett.* **71**, 3353 (1997).

¹⁶O. Tikhomirov, B. Red'kin, A. Trivelli, and J. Levy, *J. Appl. Phys.* **87**, 1932 (2000).

¹⁷O. Tikhomirov, H. Jiang, and J. Levy, *Appl. Phys. Lett.* **77**, 2048 (2000).

¹⁸F. Bai, J. Li, and D. Viehland, *J. Appl. Phys.* **97**, 054103 (2005).

¹⁹O. Tikhomirov, H. Jiang, and J. Levy, *Phys. Rev. Lett.* **89**, 147601 (2002).

²⁰X. Wan, H. Luo, X. Zhao, D. Y. Wang, H. L. W. Chan, and C. L. Choy, *Appl. Phys. Lett.* **85**, 5233 (2004); *Solid State Commun.* **134**, 547 (2005).